

Article

Impact of Environmental Factors on the Formation and Development of Biological Soil Crusts in Lime Concrete Materials of Building Facades

Wenxuan Xiong ¹, Yue Tao ¹, Panpan Wang ¹, Kaiting Wu ² and Lanzhou Chen ^{1,*}

¹ Hubei Key Laboratory of Biomass Resource Chemistry and Environmental Biotechnology, Hubei Research Center of Environment Remediation Technology, School of Resource & Environmental Sciences, Wuhan University, Wuhan 430079, China; xiongwenxuan@whu.edu.cn (W.X.); taoyue@whu.edu.cn (Y.T.); wangpanpan@whu.edu.cn (P.W.)

² Logistics Support Department, Wuhan University, Wuhan 430079, China; wkt20032003@whu.edu.cn

* Correspondence: chenlz@whu.edu.cn; Tel.: +86-027-6877-8893

Abstract: Microbial colonization leads to the formation of biological soil crusts (BSCs) on the surface of architecture, which causes the deterioration of construction materials. However, little information is available on the formation of BSCs on lime concrete materials of early architecture. In this study, the variances of microbial communities, physicochemical properties, and surrounding environmental factors of the lime concrete facades from the early architecture of Wuhan University were investigated. It was found that the surface of lime concrete materials was internally porous and permeable, embedded with biofilms of cyanobacteria, mosses, bacteria, and fungi. Redundancy analysis (RDA) analysis showed that the abundances of photoautotrophic microorganisms depended on light intensity and moisture content of construction materials, while that of heterotrophic microorganisms depended on total nitrogen (TN) and NO_3^- -N content. The deposition of total carbon (TC), NH_4^+ -N, and total organic carbon (TOC) was mainly generated by photoautotrophic microorganisms. The lime concrete surface of early architecture allowed internal growth of microorganisms and excretion of metabolites, which promoted the biodeterioration of lime concrete materials.

Keywords: biodeterioration; microbial community; lime concrete; biological soil crusts



Citation: Xiong, W.; Tao, Y.; Wang, P.; Wu, K.; Chen, L. Impact of Environmental Factors on the Formation and Development of Biological Soil Crusts in Lime Concrete Materials of Building Facades. *Appl. Sci.* **2022**, *12*, 2974. <https://doi.org/10.3390/app12062974>

Academic Editor: Panagiotis G. Asteris

Received: 18 February 2022

Accepted: 10 March 2022

Published: 15 March 2022

Publisher's Note: MDPI stays neutral with regard to jurisdictional claims in published maps and institutional affiliations.



Copyright: © 2022 by the authors. Licensee MDPI, Basel, Switzerland. This article is an open access article distributed under the terms and conditions of the Creative Commons Attribution (CC BY) license (<https://creativecommons.org/licenses/by/4.0/>).

1. Introduction

Ancient and modern cultural heritage structures deteriorate because of variable interactions between physicochemical and biological factors. Microbial activities and their effects combined with physicochemical attack are considered central to the deterioration of cultural heritage [1]. Structural damage caused by microorganisms is defined as biodeterioration. In the past few decades, biodeterioration processes in cultural heritage structures and underlying biochemical mechanisms have been elucidated [2,3]. Many microbial species are involved in biodeterioration processes [4]. The colonization and deterioration processes on matrices are usually induced by heterotrophic microorganisms and photoautotrophic microorganisms, including bacteria, cyanobacteria, algae, fungi, and mosses, the complexes formed by which are usually named biological soil crusts (BSCs) [5,6]. Biomass-rich biofilms formed by photoautotrophic organisms provide good nutritional bases for subsequent heterotrophic microbial colonization [7]. Chemoorganotrophic microorganisms are deeply involved in biochemical degradation processes, and their secretions, such as organic acids and enzymes, dissolve mineral components in matrices and precipitate salts [8]. Moreover, filamentous fungi and actinomycetes can cause biophysical damage to the matrices by expanding their hyphae [9]. Biodeterioration processes caused by various microorganisms reduce the strength and weights of construction materials, affecting the structural integrity and aesthetic appeal of the cultural heritage structures [10]. However,

there is little information about the biodeterioration of lime concrete materials, especially in the early architecture of China.

Microbial colonization is associated with the different actions of environmental factors and the physicochemical characteristics of construction materials [11]. Environmental factors, such as light intensity, temperature, and relative humidity, contribute to physical and biophysical damages [12]. Caneva et al. showed that reduction in rainfall and humidity decrease the biodeterioration of Roman monuments, demonstrating that water availability is the main limiting factor for the development of microbial populations, such as cyanobacteria, algae, and lichens [13]. In addition, physicochemical properties of construction materials, including compressive strength, water content, porosity, surface roughness, and available nutrients [14], are interrelated and affect the susceptibility of a surface to microbial colonization. Building materials with rough surfaces and high porosity provide colonization sites and favorable habitats for microorganisms by retaining water and depositing organic compounds on their surfaces. Owing to metabolic variability among microorganisms (e.g., heterotrophic microorganisms rely on organic compounds to maintain growth, whereas photoautotrophic microorganisms use CO₂ as a carbon source and light and minerals as energy sources). The mineral and organic compound composition of building materials are related to the community composition of microorganisms [15]. Nonetheless, the effects of environmental factors on BSCs formation in lime concrete materials are not elucidated.

The establishment of preventive conservation strategies for cultural heritage requires a detailed description of the impact factors and mechanisms of biodeterioration, but a lack of knowledge in regard to modern concrete cultural heritage still remains. Concrete may deteriorate due to physicochemical processes, such as freeze–thaw attack, reinforcement corrosion, and sulfate attack, which reduce the strength and weight and enhance the bioreceptivity of surfaces to severe biodeterioration [16,17]. Lime concrete is a concrete consisting of sand, lime, and gravel and had been widely used before it was replaced by Portland cement [18,19]. Lime concrete architecture is one of the most famous architectural creations in which the inherent Chinese architectural style is influenced by advanced Western construction techniques [20]. The early architecture of Wuhan University, one of the first lime concrete buildings in China, was inscribed in 2016 in the first batch of Chinese Architectural Heritage of the 20th Century List [21]. In this study, samples from the facades of some typical constructions of Wuhan University with biofouled characteristic surface were collected to investigate the effects of environmental factors and the physicochemical properties of the concrete on the composition of microbial community (bacteria, fungi, cyanobacteria, and mosses), aiming to inform the formation and development process of BSCs on the lime concrete facades and to provide a reference for the establishment of conservation strategies for concrete cultural heritage.

2. Materials and Methods

2.1. Sampling Sites

Wuhan City is located in the middle of China with a dominant northern subtropical humid monsoon climate [22]. The minimum and maximum annual average temperatures are 0.4 °C and 28.7 °C, respectively, with an average annual precipitation of 1100 mm [23]. The average annual solar brightness is approximately 2000 h, coupled with the urban heat island effect [24]. Seven lime concrete structures in the early architecture of Wuhan University with visible biofouled surface characteristics were selected. Two historical structures in Wuhan with similar styles from the same period were also inspected (S-6 and S-7). The completion dates of these buildings ranged from 1888 to 1952 [25–27], with surrounding environmental factors also recorded in Table S1. In some structures with severe biofouling signs, we collected samples from the facades in different directions to comprehensively cover the most severe cases of biocolonization on the studied structures [28]. The specific locations of the sampling sites are shown in Figure S1. As shown in Table S1 and Figure S2, Site 1 (S-1) and Site 2 (S-2) were facades of Li Da's former residence in different directions.

S-1 was exposed to direct sunlight and showed black biofilms, while S-2 was shaded by trees and showed dark green biofilms. Site 3 (S-3) had green crusts on its surface. Site 4 (S-4) and Site 5 (S-5) were the facades of the archives with different directions and discoloration, e.g., S-4 was rusty red discoloration, and S-5 was black discoloration. The surface of Site 7 (S-7) was cracking and with black biofilms, while that of Site 8 (S-8) was with obvious moss growth. Site 6 (S-6), Site 9 (S-9), Site 10 (S-10), and Site 11 (S-11) were facades that belonged to different buildings, but all showed green biofilms. Site 12 (S-12) and Site 13 (S-13) were the shaded and sunny facades of the old library, both with moist black-green biofilm growth. The physicochemical properties of construction materials affecting the microbial colonization are listed in Table 1.

Table 1. Physicochemical parameters of the materials. Results were obtained from three replicates (mean \pm standard deviation).

| Sample | Water Content (%) | TN (g·kg ⁻¹) | TC (g·kg ⁻¹) | TOC (g·kg ⁻¹) | NH ₄ ⁺ -N (mg·kg ⁻¹) | NO ₃ ⁻ -N (mg·kg ⁻¹) |
|--------|---------------------|--------------------------|--------------------------|---------------------------|--|--|
| S-1 | 13.76 \pm 0.82 de | 0.20 \pm 0.04 f | 80.60 \pm 2.69 d | 7.25 \pm 0.23 c | 19.01 \pm 1.03 de | 9.39 \pm 0.19 fg |
| S-2 | 28.98 \pm 0.65 ab | 0.35 \pm 0.01 ef | 115.15 \pm 0.35 c | 12.94 \pm 1.36 b | 26.38 \pm 0.72 bc | 18.62 \pm 0.09 d |
| S-3 | 35.96 \pm 0.78 a | 1.20 \pm 0.07 b | 82.35 \pm 3.68 e | 7.43 \pm 0.98 c | 45.76 \pm 1.74 a | 46.67 \pm 0.79 a |
| S-4 | 18.63 \pm 0.25 cd | 3.00 \pm 0.57 a | 134.50 \pm 1.41 b | 7.15 \pm 0.54 c | 11.60 \pm 0.34 fg | 15.04 \pm 1.54 de |
| S-5 | 12.59 \pm 1.83 de | 0.40 \pm 0.14 e | 147.30 \pm 1.41 a | 19.40 \pm 2.19 a | 23.50 \pm 1.38 cd | 9.62 \pm 0.19 fg |
| S-6 | 12.23 \pm 3.76 de | 0.70 \pm 0.06 d | 55.10 \pm 0.85 e | 6.15 \pm 0.35 cd | 2.67 \pm 0.36 h | 0.59 \pm 0.05 h |
| S-7 | 13.61 \pm 2.35 de | 1.30 \pm 0.02 b | 28.75 \pm 0.35 gh | 1.89 \pm 0.08 e | 7.14 \pm 0.96 gh | 24.21 \pm 0.07 c |
| S-8 | 18.60 \pm 1.83 cd | 0.40 \pm 0.06 e | 24.45 \pm 0.64 i | 3.76 \pm 0.46 de | 5.64 \pm 0.57 h | 5.24 \pm 0.22 gh |
| S-9 | 12.96 \pm 1.07 de | 1.25 \pm 0.12 b | 29.25 \pm 1.48 gh | 2.65 \pm 0.07 e | 7.12 \pm 0.49 gh | 9.85 \pm 0.18 fg |
| S-10 | 15.09 \pm 0.93 de | 0.65 \pm 0.07 d | 32.50 \pm 0.14 f | 3.44 \pm 0.07 e | 16.01 \pm 0.75 ef | 51.00 \pm 0.20 a |
| S-11 | 24.12 \pm 0.80 bc | 1.00 \pm 0.04 c | 30.90 \pm 0.99 fg | 10.71 \pm 1.36 b | 29.38 \pm 3.50 b | 35.45 \pm 0.04 b |
| S-12 | 9.79 \pm 0.01 e | 0.25 \pm 0.07 ef | 20.45 \pm 1.06 j | 2.23 \pm 0.08 e | 11.56 \pm 0.82 fg | 0.42 \pm 0.05 h |
| S-13 | 9.33 \pm 0.05 e | 1.25 \pm 0.08 b | 27.85 \pm 1.06 h | 2.18 \pm 0.02 e | 41.27 \pm 4.57 a | 11.08 \pm 1.69 ef |

Notes: Different letters (a, b, c, d, e, f, g, h and i) indicate that the difference in a given parameter is significant at the 0.05 level ($p < 0.05$).

2.2. Sample Collection

Distinct biofouled outlines were found in the sampling sites, coupled with physical damage, such as wall cracking and peeling: green biofilms, black-green discoloration, green crusting, moss growth, and rust-red tones (Figure S2). The facades of early architecture had obvious biofilms or biodeterioration marks and were selected as sample sites. Small pieces of biofilms and construction materials were collected from biocolonial-style buildings after the rainy season in July and October 2020. Biofilms were collected manually from the facade surface with a sterile blade approximately 1–2 m above the ground. Small fragments of the construction materials close to biocolonization were collected with a sterile chisel to characterize their physicochemical properties. The crust samples were collected and stored at -80 °C until DNA extraction.

2.3. DNA Extraction and Quantitative Polymerase Chain Reaction (qPCR)

FastDNA Spin Kit for Soil (MP Biomedical, California, America) was used in extracting total DNA from the biofilms according to the manufacturer's instructions. The relative abundance of bacteria, fungi, moss, cyanobacteria, and eukaryotic photoautotrophic microorganism communities was measured through quantitative polymerase chain reaction (qPCR). The V3 region of bacterial 16S rRNA gene, cyanobacterial 16S rRNA gene, moss chloroplast rps4 gene, fungal 25-28S rRNA gene, and plastid 23S rRNA gene of the eukaryotic photoautotrophic microorganisms were amplified [29]. The primer sets used are listed in Table S2.

2.4. Physicochemical Parameters Measurement of the Construction Materials

The total nitrogen (TN) and total carbon (TC) content in the construction material samples was determined with an elemental analyzer (Vario Macro Cube, Elementar, Germany). Total organic carbon (TOC) was measured with the H₂SO₄–K₂Cr₂O₇ oxidation method [30]. Inorganic N in the samples was extracted through 2M KCl solution leaching, and then

ammonium and nitrate nitrogen were determined with the colorimetric method [31]. Water content was analyzed by measuring lost weight after heat drying to constant weight at 105 °C.

2.5. Fourier-Transform Infrared (FTIR) Spectroscopy

The internal functional group of construction materials was analyzed using Fourier-transform infrared (FTIR). The spectra were recorded in a range of 4000–400 cm^{-1} at a spectral resolution of 4 cm^{-1} by using an FTIR spectrometer (Nicolet 5700, Thermo, Waltham, MA, America).

2.6. Scanning Electron Microscopy (SEM)

The microstructures of the biofilms on the construction materials were analyzed with a scanning electron microscope (Quanta, FEI, Eindhoven, The Netherlands). Three construction material samples (approximately 1 cm \times 1 cm in observed surface area) with biofilm growth from each sample site were fixed using glutaraldehyde and dehydrated in a graded ethanol series. The dehydrated samples were then gold-plated and visualized in high vacuum mode at an accelerating voltage of 20 kV. Representative figures were selected for analysis.

2.7. X-ray Diffraction (XRD)

The mineral composition of the construction materials was determined through X-ray diffraction (XRD; XPert Pro, PANalytical, Almelo, The Netherlands). The measurement was performed at 40 kV and 50 mA, with an angular range (2θ) scanned between 5° and 80° at a scan rate of 2° 2θ min^{-1} .

2.8. N₂ Physical Adsorption Analysis

The lime concrete samples were dried and degassed at 437 K under vacuum for 4 h, and the surface area and pore size were measured by N₂ adsorption tests using an automatic physical adsorption instrument (Belsorp-minII, MicrotracBEL, Osaka, Japan).

2.9. Statistical Analysis

MDI Jade 6 software with powder diffraction database was applied to the analysis of XRD results and identification of mineral phases in samples. Canonical correspondence analysis (RDA) was performed using Canoco 5 to correlate the environmental factors and community variables. Moreover, mapping and labeling were conducted on Origin Pro 2021.

3. Results

3.1. Sample Properties

The variances of physicochemical parameters of the materials from different samples are shown in Table 1. The total nitrogen (TN) content of the samples varied from 0.10 $\text{g}\cdot\text{kg}^{-1}$ to 3.0 $\text{g}\cdot\text{kg}^{-1}$, with an average of 0.92 $\text{g}\cdot\text{kg}^{-1}$. The samples of S-3 and S-4 contained higher total nitrogen (TN) content. The total carbon (TC) content ranged from 20.45 $\text{g}\cdot\text{kg}^{-1}$ to 147.30 $\text{g}\cdot\text{kg}^{-1}$, with a mean value of 62.24 $\text{g}\cdot\text{kg}^{-1}$. The total organic carbon (TOC) content of the samples ranged from 1.89 $\text{g}\cdot\text{kg}^{-1}$ to 19.4 $\text{g}\cdot\text{kg}^{-1}$, with an average of 6.71 $\text{g}\cdot\text{kg}^{-1}$. The samples from S-4 and S-5 contained higher total carbon (TC) content, while the samples from S-2 and S-5 contained higher total organic carbon (TOC) content. Sample sites S-4 and S-5 had distinct thick biofilms on the structure surfaces, and these biofilms may be related to the high total carbon (TC) and total organic carbon (TOC) levels of the materials. The average values of NH_4^+ -N and NO_3^- -N were 19 and 18 $\text{mg}\cdot\text{kg}^{-1}$, respectively. The mean water content of the construction materials was considered high (17.96%) because of air-conditioning equipment drainage, garden irrigation, rainwater gutter dumping, and humid climate.

3.2. Mineralogical Composition of Lime Concrete

The mineral composition of the concrete was evaluated by performing X-ray diffraction (XRD) and analysis of the diffraction pattern obtained by accelerated electron bombardment of the sample. The XRD diffractograms of the samples from different sample sites are shown in Figure S4. The main crystalline phases of the concrete were quartz and calcite and contained magnesian calcite, anorthite, and albite, as shown in Table 2 and Figure S4. Dolomite was found in S-1, S-2, and S-11, and a small amount of muscovite was found in S-8. S-9 was the only sample site where whewellite was identified (Figure 1A). Many sample sites had kaolinite (S-3 and S-4) and gypsum (S-3, S-9, S-10, and S-13). S-5 was the only site where thaumasite was identified (Figure 1A).

Table 2. Mineral composition of the construction materials. “X” indicates the presence of the mineral at the sample site, while “—” indicates the absence of the mineral.

| Samples | Calcite | Quartz | Calcite, Magnesian | Albite | Dolomite | Gypsum | Kaolinite | Others |
|---------|---------|--------|--------------------|--------|----------|--------|-----------|------------|
| S-1 | X | X | X | — | X | — | — | — |
| S-2 | X | X | X | — | X | — | — | — |
| S-3 | X | X | X | — | — | X | X | — |
| S-4 | X | X | — | — | — | — | X | — |
| S-5 | X | X | — | — | — | — | — | Thaumasite |
| S-6 | X | X | X | — | — | — | — | — |
| S-7 | X | X | — | — | — | — | — | Orthoclase |
| S-8 | X | X | — | X | — | — | — | Muscovite |
| S-9 | X | X | — | X | — | X | — | Whewellite |
| S-10 | X | X | — | X | — | X | — | — |
| S-11 | X | X | — | — | X | — | — | — |
| S-12 | X | X | — | — | — | — | — | Anorthite |
| S-13 | X | X | — | — | — | X | — | — |

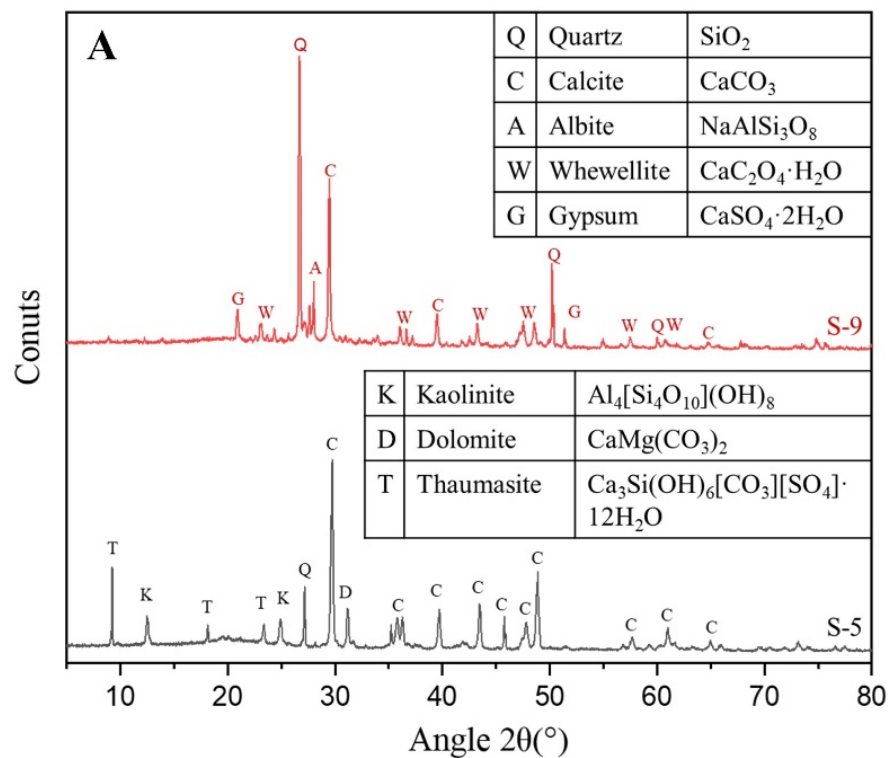


Figure 1. Cont.

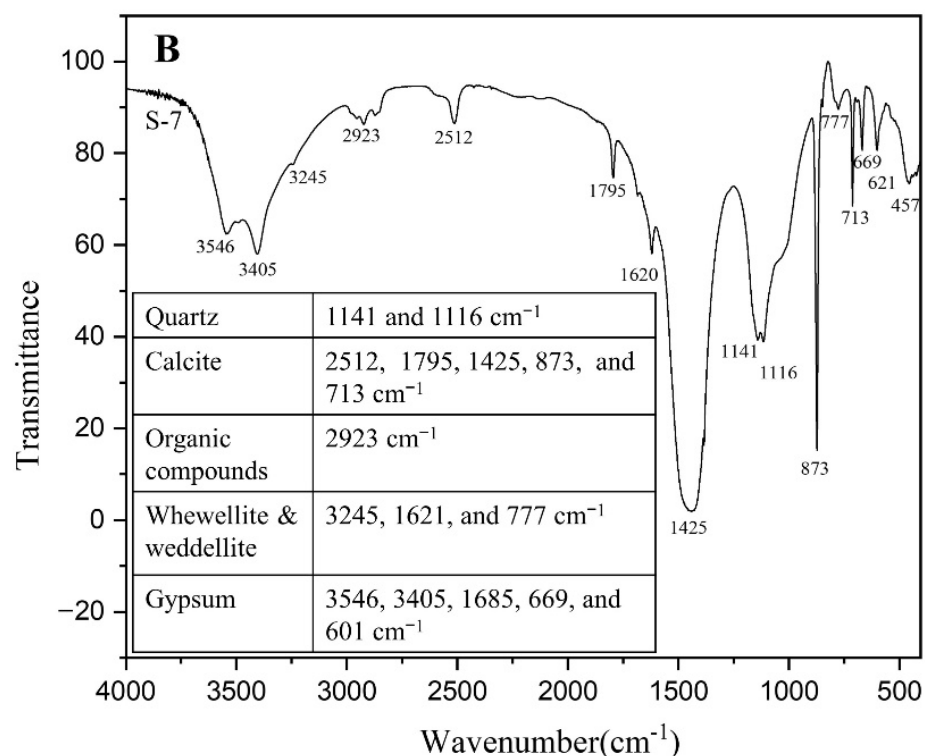


Figure 1. (A) XRD diffractograms of sample S-5 and S-9 with evident biodeterioration signs. (B) FTIR analysis of sample S-7 showing its functional groups and molecular bonds.

We performed FTIR analysis to complement the results and obtain information about the functional groups of the construction materials. The FTIR analysis of the samples from different sample sites are shown in Figure S5. In all the samples, calcite (bands at 2512, 1795, 1425, 873, and 713 cm^{-1}) and quartz (band around 1100 cm^{-1}) were identified. S-7 had the most abundant functional groups of organic materials and degradation products (Figure 1B). The FTIR spectrum bands at 3245, 1621, and 777 cm^{-1} corresponded to calcium oxalate (whewellite and weddellite), whereas those at 3546, 3405, 1685, 669, and 601 cm^{-1} corresponded to calcium sulfate dihydrate (gypsum). The band around 2920 cm^{-1} highlighted the presence of organic compounds.

3.3. Microbial Colonization Patterns on Lime Concrete

Scanning electron microscopy (SEM) observations revealed the structural features of the concrete surface and microbiological contamination. The lime concrete was characterized by high porosity (Figure 2C) and air void formation induced by the concrete mixing process (Figure 2B). The pores were 50–200 μm in diameter. The sand or gravel used as aggregates in the concrete was visible (Figure 2A,B). Samples were extracted from the facades of the cultural heritage and contained microcracks on their surface because of weathering and erosion over time (Figure 2D,J). Biological contamination occurred in various forms, including filamentous microorganisms (Figure 2D–G,K), reticulate biofilms (Figure 2H–J), and clusters formed by spherical microbes (Figure 2L). Biofilms were identified extensively in the vicinity of air voids and microcracks (Figure 2D–F). It is notable that the adherence of concrete fragments to the biofilms was frequently observed (Figure 2D,G–I). Morphological analysis also highlighted the extensive expansion of biofilms and widespread penetration of hyphae in the concrete interior (Figure 2F,J). Erosion was observed at the concretization of the gravel aggregate to the concrete (Figure 2A).

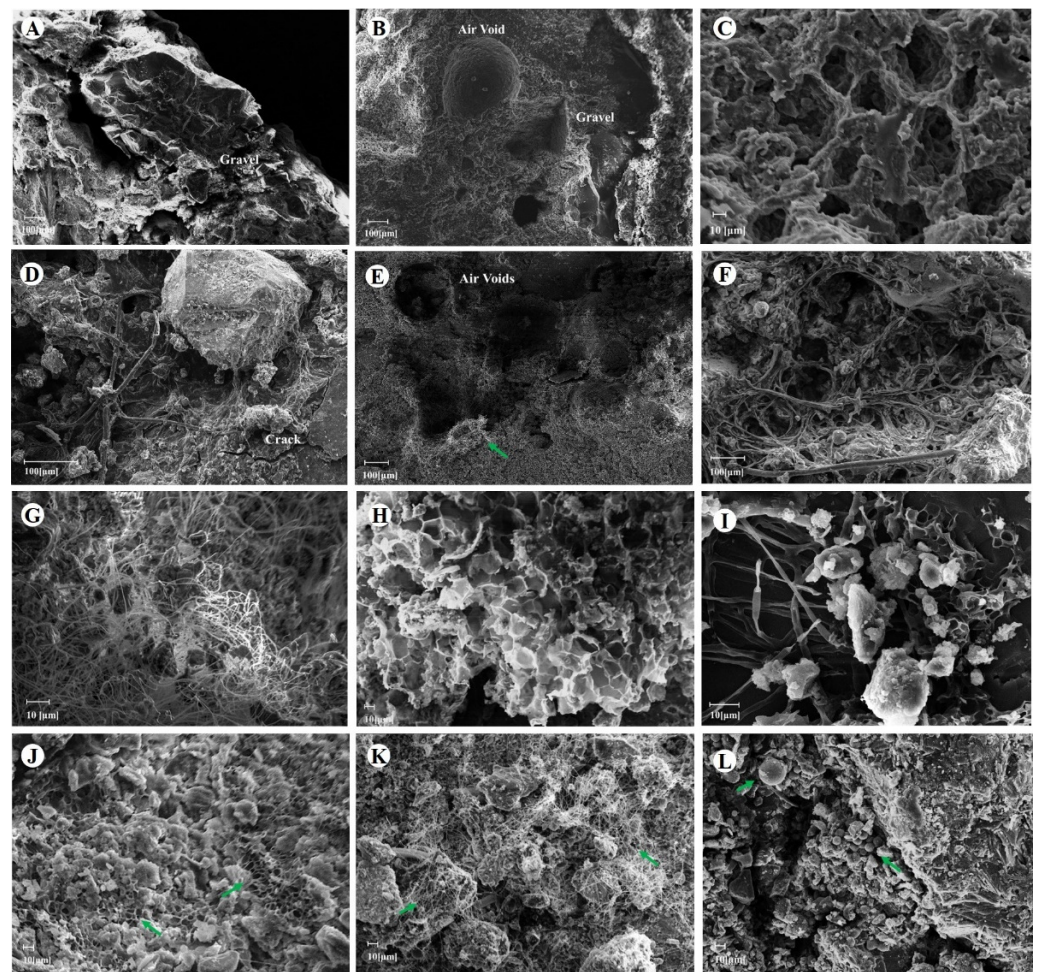


Figure 2. Scanning electron microscopy (SEM) micrographs revealing the structural features of the concrete surface (A–C) and biofilm formations on their surface (D–L).

3.4. Variances of Microbial Community Composition

Microbial abundance of the early building facades of Wuhan University was measured by quantitative polymerase chain reaction (qPCR). The gene copies per gram of dry materials of cyanobacterial 16S rRNA gene, moss chloroplast *rps4*, bacterial 16S rRNA, fungal 25-28S rRNA, and plastid 23S rRNA of eukaryotic photoautotrophic microorganisms were quantified through qPCR (Figure 3). The content of bacterial 16S rRNA ranged from 8.64×10^6 to 2.50×10^9 copies, and the content of fungal 25-28S rRNA ranged from 5.43×10^4 copies to 8.41×10^8 copies. Cyanobacterial 16S rRNA gene and moss chloroplast *rps4* gene copies ranged from 3.06×10^2 copies to 4.78×10^7 copies and from 2.46×10^4 copies to 2.25×10^7 copies, respectively. The gene copies of the plastid 23S rRNA gene, which represented the population of eukaryotic photoautotrophs, ranged from 3.51×10^4 copies to 9.88×10^8 copies. In biofilms of S-2, S-3, S-4, S-6, S-7, S-8, and S-13, the abundance of eukaryotic photoautotrophs was the highest among these microbial communities. Bacteria had the highest abundance in the microbial communities of S-5 and S-9, while in the biofilms of S-10, S-11, and S-12, the abundance of fungi was the highest among these microbial communities.

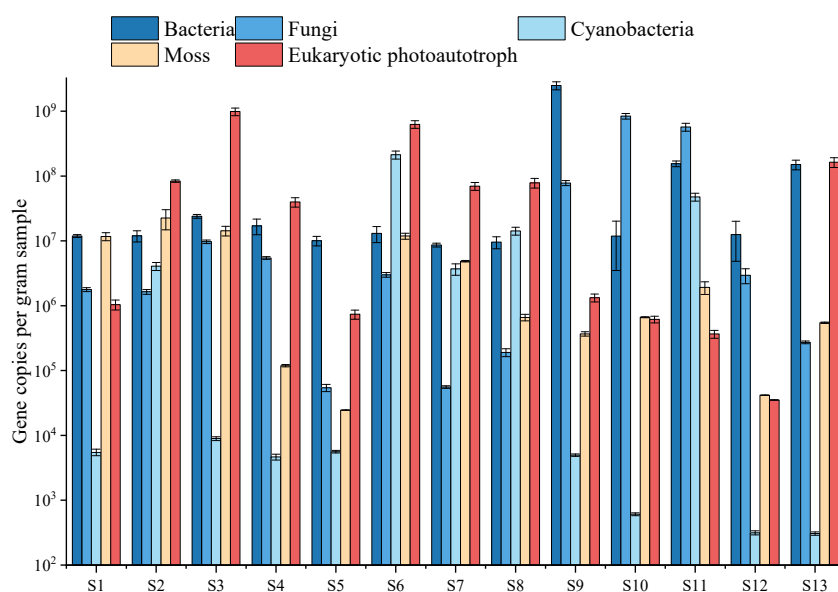


Figure 3. Abundance of bacterial 16S rRNA, fungal 25-28S rRNA, cyanobacterial 16S rRNA gene, moss chloroplast rps4, and plastid 23S rRNA of eukaryotic photoautotrophic microorganisms in 13 sites of the early architecture of Wuhan University.

3.5. Correlations between Physicochemical Parameters and Microbial Community Abundance

Redundancy analysis (RDA) was conducted to display the correlations between the physicochemical properties of concrete and surrounding environmental factors with microbial community abundance. As shown in Figure 4A, Axis1 explained 50.52% of the total variance, whereas Axis2 explained 9.87%. The abundance of mosses, cyanobacteria, and eukaryotic photoautotrophs was positively correlated with the water content of the matrix and negatively correlated with shading. Moreover, total carbon (TC), total organic carbon (TOC), and NH₄⁺-N content was positively correlated with the population abundance of mosses, cyanobacteria, and eukaryotic photoautotrophs. The abundance of fungal and bacterial populations was positively correlated with the NO₃⁻-N and total nitrogen (TN) content, respectively. Figure 4B showed that the total carbon (TC), total organic carbon (TOC), and NH₄⁺-N content of the matrix explained 15%, 8.2%, and 7.8% of the total variations in microbial communities, respectively. The shading levels and the water content of the concrete explained 13.6% and 9.1% of the total variation, respectively.

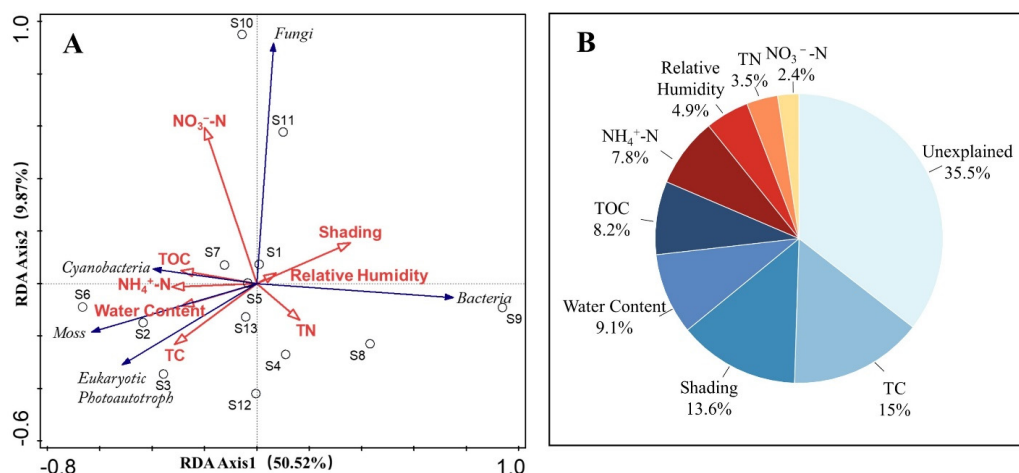


Figure 4. (A) Redundancy analysis (RDA) deciphering the correlations between microbial populations abundance and physicochemical parameters. (B) Percentages of the total variation in microbial communities explained by concrete properties and environmental factors.

4. Discussion

4.1. Bioreceptivity of Concrete Affected by Environmental Factors

XRD and FTIR results demonstrated that the concrete samples were enriched with mineral phases, including calcite, quartz, albite, dolomite, orthoclase, muscovite, and anorthite, which assist in the growth of microorganisms [32]. Moreover, the sampling sites selected in this study are in Central City, which is considerably affected by atmospheric pollutants. The high total organic carbon (TOC) content in the materials shown in Table 1 was likely to be derived from the accumulation of organic matter on the rough and porous surface of the concrete. The accumulation of organic atmospheric particles (polycyclic aromatic hydrocarbons, fly ash, and soot) on construction materials has been reported by Andreolli et al. [33]. The deposition of organic pollutants on surfaces facilitated the early development of microbial communities, and atmospheric pollutants were captured and accumulated by biofilms after the formation of structurally stable biofilms [34]. In addition to atmospheric pollutant sources, organic carbon in the material was likely biologically introduced. The compositional analysis in Figure 1 and Table 1 showed that the concrete was mainly inorganic, and the high total organic carbon (TOC) content may reveal the presence of surface microorganisms. As described in Section 3.3, many microorganisms penetrated the substrate, and these organisms, dead biomass, and metabolites are potential sources of organic carbon [35]. The positive correlation between photoautotrophic microorganisms and total organic carbon (TOC) presented in Figure 4 showed that total organic carbon (TOC) accumulation on the concrete surface was mainly introduced by photoautotrophic microorganisms, and the photoautotrophic microbial biomass and metabolic activities contributed to the bioreceptivity of the concrete surface.

Concrete is a porous material, most of the pores in lime concrete were mesopores with pore sizes of 2–50 nm, and few macropores with pore sizes greater than 50 nm were found (Figure S3). These pores make lime concrete capable of absorbing water from the atmosphere through its internal pores, thus improving the conditions of living organisms at the beginning of colonization [34]. Additionally, the biofilm layer became wet because of air humidity, rainfall, and surrounding human activities and because of the colonization of microorganisms on the concrete surface, and it subsequently absorbed water and prevented it from evaporating. The concrete below retained water for longer periods and supported deep microbial colonization. As shown in Table 1, the selected lime concrete generally had a higher water content due to the high porosity of the concrete and the additional water retention provided by the biofilm. This water can seriously affect the strength and aesthetic appeal of structures [36,37]. Enhanced water retention can intensify the freeze–thaw cycle of concrete and aggravate reduction in the mechanical properties and durability of concrete [38]. Moreover, when the environment turned relatively dry, soluble salts and mineral crystals from water crystallized and produced internal expansion stress on the concrete, leading to cracking, flaking, scaling, or detachment of structures. The visible growth of black or green biofilms and spreading of cracks from the lower parts upward were observed on the surface of the early architecture of Wuhan University (Figure S2). Liu et al. have described that water damage immigrates upward into the monuments, suggesting that it was caused by salts migration [37]. In the case of the early architecture of Wuhan University, the upward migration of water not only caused damage to the integrity of the concrete but also created conditions conducive to microorganisms.

The high porosity of lime concrete internally was further confirmed by morphological analysis in Figure 2. The bioreceptivity of the material correlated well with the porosity and roughness of the surface [39]. Filamentous fungi and algae adhered easily to rough surfaces. Macroscopically and microscopically, the lime concrete selected for the present study featured a highly rough surface. Therefore, the concrete surface contained abundant filamentous microorganisms (Figure 2D,F,G). Moreover, cracks due to long-term weathering were conducive to the deposition of microorganisms (Figure 2D,J). The rough surfaces, high porosity, and internal cracks of concrete provide many suitable deposition sites for airborne microorganisms, allowing surface deposition and the internal growth of various

microorganisms, including bacteria, fungi, and photoautotrophic microorganisms [40]. Photoautotrophic microorganisms assimilate CO₂ and N₂ to organic substances through photosynthesis and nitrogen fixation, which facilitate colonization by chemoautotrophs and heterotrophic microorganisms. The metabolic activities and succession processes of multiple microbial populations provide a balanced microbial community [41]. Microbial cells can be attached to extracellular polymers (EPSs) secreted by microorganisms and form biofilms with stable structures and complete biochemical functions. These biofilms prevent water evaporation, accumulate atmospheric pollutants, enhance the adhesion of microorganisms on the surface of structures, and ensure the stable development of microbial communities [42].

4.2. Effect of Microbial Colonization on Structures

Deterioration of concrete is a complex process involving biophysical and biochemical interactions. The building surfaces in this study typically showed extensive discoloration in dark green and black, occasional rust-red tones, and green encrustations (Figure S2). The discoloration of building surfaces can be induced by the deposition of atmospheric pollutants and the excretion of biogenic pigments, initially leading to the aesthetic appearance issue. The common dark green color on the surface of the early architecture of Wuhan University is likely caused by photoautotrophic microorganisms. Photoautotrophic microorganisms, such as algae and cyanobacteria, can produce pigments. As morphologically diverse prokaryotic photoautotrophic microorganisms, cyanobacteria can synthesize pigments, including phycobilin and chlorophyll α [43]. Photoautotrophic microorganisms, especially cyanobacteria, have the highest species richness in the green and blue biofilms of Angkor Wat [44]. The black and rust-red coloration of the surface from the early architecture of Wuhan University can be attributed to the actions of heterotrophic microorganisms and cyanobacteria. Fungi and actinobacteria are considered the most important biodeteriorative organisms. Fungi can produce various pigments, such as melanin, α -carotene, and β -carotene [45,46]. Melanin produced by actinomycetes is responsible for the formation of black spots in structures [47]. The brown discoloration of paint surfaces has been reported to originate from minerals, fungi, and specific cyanobacteria [48]. In addition to microorganisms, the EPS in biofilm not only adheres to cells but also traps atmospheric dust and carbon residues from automobile traffic and pigments and minerals produced by microorganisms and contributes to the discoloration of buildings [49,50].

In addition to pigments, microorganisms can produce organic acids and enzymes that trigger the biochemical corrosion of substratum material [51]. Microbial communities in the study area may produce oxalic acid and sulfuric acid, leading to the occurrence of secondary minerals, including gypsum, thaumasite, and weddellite, on the surfaces of early architecture at Wuhan University. These secondary minerals crystallize under the effects of cyclic wetting and drying, creating internal stresses in the material and resulting in cracking, flaking, scaling, or detachment of construction material.

The occurrence of gypsum and thaumasite was a result of the deposition by acidic air pollutants or biogenic sulfuric acid on structure facades, and deposition is commonly accompanied by the dissolution of calcareous construction materials [52]. As described in 3.2, relatively large amounts of gypsum, a typical deterioration product of calcareous construction materials, were found at four sampling sites [53,54]. The corroding layer produced by the gypsum on the concrete surface can penetrate concrete, occupying a large space and generating stress because of the large density difference between gypsum and the concrete, and eventually leading to cracking, detachment, and destruction of external walls [55]. Additionally, some microorganisms require a certain amount of sulfur as a macronutrient [56]. Ortega-Calvo et al. proved that gypsum can be a source of sulfur for microbial growth [57]. The production of gypsum not only affected the structural integrity of the concrete but also provided additional nutrients to microorganisms. Moreover, the occurrence of thaumasite in S-5 represented the thaumasite form of sulfate attack (TSA), which has attracted considerable interest in the past few decades as a newly discovered

pattern of sulfate erosion of concrete. Unlike conventional sulfate attack, which leads to the expansion and destruction of concrete, TSA leads to a more insidious and destructive transformation of a concrete matrix inward to an incohesive mass from the surface inward [58]. These sulfate attack processes resulted in reduced strength, altered composition, and increased surface area of concrete.

The presence of weddellite in S-9 is associated with the metabolic activity of microorganisms and could cause biophysical damage to the structures. Calcium oxalate is the most insoluble oxalate and often found in living organisms and nature in the form of whewellite ($\text{CaC}_2\text{O}_4 \cdot \text{H}_2\text{O}$) and weddellite ($\text{CaC}_2\text{O}_4 \cdot 2\text{H}_2\text{O}$) [59]. The biosynthesis of calcium oxalate can be presented by this equation: $\text{Ca}^{2+} + \text{C}_2\text{O}_4^{2-} + x\text{H}_2\text{O} \rightarrow \text{Ca}(\text{C}_2\text{O}_4) \cdot x\text{H}_2\text{O}(\text{s}) \downarrow$. However, some studies suggested that the precipitation of calcium oxalate is negligible or even beneficial because insoluble oxalate crystals can block pores and act as diffusion barriers, thus limiting the further leaching of calcium [60]. However, the precipitation of significant amounts of calcium oxalate occurring in mineral-based building materials is inclined to cause physicochemical damage. The complexation of oxalic acid with calcium ions causes the dissolution of matrices, and the expansion of secondary oxalate biominerals causes physical damage [61]. The presence of whewellite and weddellite is frequently found in the black and patina crusts of limestone and concrete building surfaces [62]. Fungal-induced whewellite and weddellite precipitation can form biomineralized crusts with dead hyphae [63]. Although the amount of weddellite found in S-9 is comparatively low, high levels of weddellite can cause crusting and discoloration in buildings because of the constant input of oxalic acid from surface microbial communities.

Corrosion by biogenic acids and the crystallization of secondary minerals decrease the strength of building material, and together with rough surfaces (as discussed in Section 4.1), facilitate the colonization of filamentous microorganisms. Importantly, in addition to the distribution of microorganisms on matrix surfaces, microorganisms can thrive in cracks and air voids (Figure 2D–F,J). The internal expansion of microorganisms and penetration of concrete by hyphae may induce cracks and enlarge current cracks and pores and thereby increase the porosity and connectivity of material, even leading to the detachment of some fragments. These effects were indicated by the material debris attached to the biofilm (Figure 2G,H). This phenomenon causes biophysical damage to concrete and eventually leads to the dissolution and disintegration of concrete.

4.3. Microbial Communities Affected by Environmental Factors

Applied multianalytical methodology enabled us to identify the correlation of microbial abundance with the physical–chemical properties of substrates and environmental factors. As described in 3.5, owing to the positive correlation of population abundance with the moisture content of concrete and negative correlation with shading, water availability and light intensity were identified as key factors for the development of photoautotrophic microorganisms, including mosses, cyanobacteria, and eukaryotic photoautotrophs. The total carbon (TC), total organic carbon (TOC), and NH_4^+ -N content was positively correlated with the population abundance of mosses, cyanobacteria, and eukaryotic photoautotrophs, demonstrating that the organic nutrients of the concrete were mainly derived from the photoautotrophic microorganisms. Both metabolites and the biomass of photoautotrophic microorganisms are potential carbon and nitrogen sources [64,65]. As shown in Section 3.2, the compositional analysis showed that concrete was mainly composed of inorganic compounds with low availability. Thus, photosynthesis and nitrogen fixation by photoautotrophic microorganisms contribute importantly to the microbial community development on the surfaces of inorganic building materials. This was also supported by the study of Gaylarde et al., who treated structure facades with algicides to remove photoautotrophic microorganisms and inhibit the growth of fungi and bacteria [66]. These results indicated the key role of photoautotrophic microorganisms in the biocolonization processes on the surface of inorganic materials such as concrete and stone.

5. Conclusions

In this work, a multidisciplinary methodology combining material science and molecular biological analysis was used to investigate the variances of microbial communities and physicochemical properties of lime concrete facades of the early architecture of Wuhan University in response to environmental factors. Lime concrete growing biofilm contained higher content of total carbon (TC), total organic carbon (TOC), and NH_4^+ -N, and it was also enriched with mineral components including calcite, quartz, albite, dolomite, orthoclase, muscovite, and anorthite. In addition, the rough surface, high porosity, and microcracks of lime concrete provided deposition sites for microorganisms. The synergistic interaction of these physicochemical properties of lime concrete and environmental factors constituted a microenvironment suitable for microbial growth. The internal expansion of biofilms caused biophysical damage to the concrete. The metabolic activity of microorganisms also caused the production of deterioration products including gypsum, thaumasite, and weddellite, resulting in biochemical damage to the matrix.

Redundancy analysis (RDA) analysis showed the deposition of total carbon (TC), NH_4^+ -N, total organic carbon (TOC) on the lime concrete were derived from the metabolic of photoautotrophic microorganisms, illustrating the key role of photoautotrophic microorganisms in the biodeterioration process of lime concrete. The biomass of photoautotrophic microorganisms depends on the light intensity and moisture content of building materials, while the abundance of heterotrophic microorganisms depends on TN and NO_3^- -N content.

Overall, this study is the first report on the origin of lime concrete bioreceptivity. The results obtained from this study could represent a pioneering advance of the relation of physical–chemical characteristics of the lime concrete material and environmental factors with the types of microorganisms associated with the triggering of biodeterioration processes, with a contribution to the subsequent development of cultural heritage conservation strategies.

Supplementary Materials: The following supporting information can be downloaded at: <https://www.mdpi.com/article/10.3390/app12062974/s1>, Figure S1: Location of sampling sites; Figure S2: Biofilms on the facades of the early architecture of Wuhan University; Figure S3: Pore volume and pore size distribution of lime concrete; Figure S4: XRD diffractograms of the construction materials; Figure S5: FTIR analysis of the construction materials; Table S1: Details of the historical constructions and surrounding environmental factors, Table S2: Primer sets used in this study for bacteria, fungi, cyanobacteria, moss, and eukaryotic photoautotroph.

Author Contributions: Conceptualization, L.C. and Y.T.; methodology, W.X.; software, P.W.; resources, K.W.; writing—original draft preparation, W.X.; writing—review and editing, L.C. and W.X.; project administration, L.C. All authors have read and agreed to the published version of the manuscript.

Funding: This research was funded by the National Natural Science Foundation of China, Grant Number 31870432.

Institutional Review Board Statement: Not applicable for studies not involving humans or animals.

Informed Consent Statement: Not applicable for studies not involving humans.

Data Availability Statement: Data are contained within the article or Supplementary Materials.

Conflicts of Interest: The authors declare no conflict of interest.

References

1. Saiz-Jimenez, C. Biodeterioration vs biodegradation: The role of microorganisms in the removal of pollutants deposited on historic buildings. *Int. Biodeter. Biodegr.* **1997**, *40*, 225–232. [[CrossRef](#)]
2. Meng, H.; Luo, L.; Chan, H.W.; Katayama, Y.; Gu, J. Higher diversity and abundance of ammonia-oxidizing archaea than bacteria detected at the Bayon Temple of Angkor Thom in Cambodia. *Int. Biodeter. Biodegr.* **2016**, *115*, 234–243. [[CrossRef](#)]
3. Leplat, J.; Bousta, F.; Francois, A.; Guiavarc'h, M.; Mertz, J.; Brissaud, D. The pink staircase of Sully-sur-Loire castle: Even bacteria like historic stonework. *Int. Biodeter. Biodegr.* **2019**, *145*, 104805. [[CrossRef](#)]

4. Beata, G. The use of -omics tools for assessing biodeterioration of cultural heritage: A review. *J. Cult. Herit.* **2020**, *45*, 351–361. [[CrossRef](#)]
5. Ariño, X.; Saiz-Jimenez, C. Colonization and deterioration processes in Roman mortars by cyanobacteria, algae and lichens. *Aerobiologia* **1996**, *12*, 9–18. [[CrossRef](#)]
6. Adessi, A.; Cruz De Carvalho, R.; De Philippis, R.; Branquinho, C.; Marques Da Silva, J. Microbial extracellular polymeric substances improve water retention in dryland biological soil crusts. *Soil Biol. Biochem.* **2018**, *116*, 67–69. [[CrossRef](#)]
7. Crispim, C.; Gaylarde, C. Cyanobacteria and biodeterioration of cultural heritage: A review. *Microb. Ecol.* **2005**, *49*, 1–9. [[CrossRef](#)]
8. De Windt, L.; Devillers, P. Modeling the degradation of Portland cement pastes by biogenic organic acids. *Cem. Concr. Res.* **2010**, *40*, 1165–1174. [[CrossRef](#)]
9. Wiktor, V.; De Leo, F.; Urzi, C.; Guyonnet, R.; Grosseau, P.; Garcia-Diaz, E. Accelerated laboratory test to study fungal biodeterioration of cementitious matrix. *Int. Biodeter. Biodegr.* **2009**, *63*, 1061–1065. [[CrossRef](#)]
10. De Belie, N. Microorganisms versus stony materials: A love-hate relationship. *Mater. Struct.* **2010**, *43*, 1191–1202. [[CrossRef](#)]
11. Hayek, M.; Salgues, M.; Souche, J.; Cunge, E.; Giraudel, C.; Paireau, O. Influence of the Intrinsic Characteristics of Cementitious Materials on Biofouling in the Marine Environment. *Sustainability* **2021**, *13*, 2625. [[CrossRef](#)]
12. Stanaszek-Tomal, E. Environmental Factors Causing the Development of Microorganisms on the Surfaces of National Cultural Monuments Made of Mineral Building Materials-Review. *Coatings* **2020**, *10*, 1203. [[CrossRef](#)]
13. Caneva, G.; Gori, E.; Montefinale, T. Biodeterioration of monuments in relation to climate changes in Rome between 19–20th centuries. *Sci. Total Environ.* **1995**, *167*, 205–214. [[CrossRef](#)]
14. Giannantonio, D.J.; Kurth, J.C.; Kurtis, K.E.; Sobczyk, P.A. Effects of concrete properties and nutrients on fungal colonization and fouling. *Int. Biodeter. Biodegr.* **2009**, *63*, 252–259. [[CrossRef](#)]
15. Adamiak, J.; Otlewska, A.; Gutarowska, B. Halophilic microbial communities in deteriorated buildings. *World J. Microb. Biot.* **2015**, *31*, 1489–1499. [[CrossRef](#)]
16. Santos, T.; Nunes, L.; Faria, P. Production of eco-efficient earth-based plasters: Influence of composition on physical performance and bio-susceptibility. *J. Clean. Prod.* **2017**, *167*, 55–67. [[CrossRef](#)]
17. Gencil, O.; Benli, A.; Bayraktar, O.Y.; Kaplan, G.; Sutcu, M.; Elabade, W.A.T. Effect of waste marble powder and rice husk ash on the microstructural, physico-mechanical and transport properties of foam concretes exposed to high temperatures and freeze-thaw cycles. *Constr. Build. Mater.* **2021**, *291*, 123374. [[CrossRef](#)]
18. Binal, A. Investigation of Hydraulic Binding Characteristics of Lime Based Mortars Used in Historical Masonry Structures. *IOP Conf. Ser. Mater. Sci. Eng.* **2017**, *245*, 22081. [[CrossRef](#)]
19. Urquhart, D.C.M. The early concrete bridges of Scotland: A heritage at risk? *J. Archit. Conserv.* **2020**, *26*, 201–214. [[CrossRef](#)]
20. Zhao, B.; Wu, J. Research on the Construction Technology of Modern History Buildings in Wuhan University. *Huazhong Archit.* **2013**, *31*, 114–121.
21. Kaihao, W. 20th Century Heritage List Salutes Chinese Structures. Available online: http://english.www.gov.cn/news/top_news/2016/09/30/content_281475455132820.htm (accessed on 14 December 2021).
22. Li, X.; Li, B.; Chen, H. Study on the relationship between urban land sprawl extension and urban thermal environment—Taking Wuhan city as an example. *Theor. Appl. Climatol.* **2019**, *137*, 1135–1148. [[CrossRef](#)]
23. Wang, L.; Gong, W.; Ma, Y.; Hu, B.; Zhang, M. Photosynthetically active radiation and its relationship with global solar radiation in Central China. *Int. J. Biometeorol.* **2014**, *58*, 1265–1277. [[CrossRef](#)] [[PubMed](#)]
24. Li, K.; Yu, Z. Comparative and Combinative Study of Urban Heat Island in Wuhan City with Remote Sensing and CFD Simulation. *Sensors* **2008**, *8*, 6692–6703. [[CrossRef](#)] [[PubMed](#)]
25. Tang, R. Consideration on the Protection of Historical Buildings—A Case Study of Modern Public Mansions in Wuhan. *J. Hubei Radio Telev. Univ.* **2019**, *39*, 54–58.
26. Tong, Q.; Zha, Y.; Li, Y. Research on Restoration and Protection of an Early Architecture of Wuhan University the College of Science. *New Archit.* **2019**, *29*, 106–110.
27. Tong, Q.; Tang, L.; Li, Q. Analysis of new campus planning for Wuhan University in the early Republic of China (1929–1937). *J. Asian Archit. Build.* **2020**, *21*, 34–47. [[CrossRef](#)]
28. Trovão, J.; Portugal, A.; Soares, F.; Paiva, D.S.; Mesquita, N.; Coelho, C.; Pinheiro, A.C.; Catarino, L.; Gil, F.; Tiago, I. Fungal diversity and distribution across distinct biodeterioration phenomena in limestone walls of the old cathedral of Coimbra, UNESCO World Heritage Site. *Int. Biodeter. Biodegr.* **2019**, *142*, 91–102. [[CrossRef](#)]
29. Deng, S.; Wang, C.; De Philippis, R.; Zhou, X.; Ye, C.; Chen, L. Use of quantitative PCR with the chloroplast gene *rps4* to determine moss abundance in the early succession stage of biological soil crusts. *Biol. Fert. Soils* **2016**, *52*, 595–599. [[CrossRef](#)]
30. Deng, S.; Ke, T.; Li, L.; Cai, S.; Zhou, Y.; Liu, Y.; Guo, L.; Chen, L.; Zhang, D. Impacts of environmental factors on the whole microbial communities in the rhizosphere of a metal-tolerant plant: *Elsholtzia haichowensis* Sun. *Environ. Pollut.* **2018**, *237*, 1088–1097. [[CrossRef](#)]
31. Wang, J.; Bao, J.; Su, J.; Li, X.; Chen, G.; Ma, X. Impact of inorganic nitrogen additions on microbes in biological soil crusts. *Soil Biol. Biochem.* **2015**, *88*, 303–313. [[CrossRef](#)]
32. Gallego-Cartagena, E.; Morillas, H.; Maguregui, M.; Patino-Camelo, K.; Marcaida, I.; Morgado-Gamero, W.; Silva, L.F.O.; Manuel Madariaga, J. A comprehensive study of biofilms growing on the built heritage of a Caribbean industrial city in correlation with construction materials. *Int. Biodeter. Biodegr.* **2020**, *147*, 104874. [[CrossRef](#)]

33. Andreolli, M.; Lampis, S.; Bernardi, P.; Calo, S.; Vallini, G. Bacteria from black crusts on stone monuments can precipitate CaCO₃ allowing the development of a new bio-consolidation protocol for ornamental stone. *Int. Biodeter. Biodegr.* **2020**, *153*, 105031. [[CrossRef](#)]
34. Liu, X.; Koestler, R.J.; Warscheid, T.; Katayama, Y.; Gu, J. Microbial deterioration and sustainable conservation of stone monuments and buildings. *Nat. Sustain.* **2020**, *3*, 991–1004. [[CrossRef](#)]
35. Baran, R.; Brodie, E.L.; Mayberry-Lewis, J.; Hummel, E.; Da Rocha, U.N.; Chakraborty, R.; Bowen, B.P.; Karaoz, U.; Cadillo-Quiroz, H.; Garcia-Pichel, F.; et al. Exometabolite niche partitioning among sympatric soil bacteria. *Nat. Commun.* **2015**, *6*, 8289. [[CrossRef](#)] [[PubMed](#)]
36. Prieto, B.; Vázquez-Nion, D.; Fuentes, E.; Durán-Román, A.G. Response of subaerial biofilms growing on stone-built cultural heritage to changing water regime and CO₂ conditions. *Int. Biodeter. Biodegr.* **2020**, *148*, 104882. [[CrossRef](#)]
37. Liu, X.; Meng, H.; Wang, Y.; Katayama, Y.; Gu, J. Water is a critical factor in evaluating and assessing microbial colonization and destruction of Angkor sandstone monuments. *Int. Biodeter. Biodegr.* **2018**, *133*, 9–16. [[CrossRef](#)]
38. Liu, H.; Luo, G.; Wei, H.; Yu, H. Strength, Permeability, and Freeze-Thaw Durability of Pervious Concrete with Different Aggregate Sizes, Porosities, and Water-Binder Ratios. *Appl. Sci.* **2018**, *8*, 1217. [[CrossRef](#)]
39. Guillitte, O.; Dreesen, R. Laboratory chamber studies and petrographic analysis as bioreceptivity assessment tools of building-materials. *Sci. Total Environ.* **1995**, *167*, 365–374. [[CrossRef](#)]
40. Sawadogo, A.Y.F.; Roux, S.; Lecomte, A. Bioreceptivity of Portland and calcium Sulphoaluminate cements in urban sewerage networks. *Constr. Build. Mater.* **2021**, *293*, 123425. [[CrossRef](#)]
41. Ling, A.L.; Robertson, C.E.; Harris, J.K.; Frank, D.N.; Kotter, C.V.; Stevens, M.J.; Pace, N.R.; Hernandez, M.T. High-Resolution Microbial Community Succession of Microbially Induced Concrete Corrosion in Working Sanitary Manholes. *PLoS ONE* **2015**, *10*, e0116400. [[CrossRef](#)]
42. Zhang, P.; Fang, F.; Chen, Y.; Shen, Y.; Zhang, W.; Yang, J.; Li, C.; Guo, J.; Liu, S.; Huang, Y.; et al. Composition of EPS fractions from suspended sludge and biofilm and their roles in microbial cell aggregation. *Chemosphere* **2014**, *117*, 59–65. [[CrossRef](#)] [[PubMed](#)]
43. Lan, W.; Li, H.; Wang, W.; Katayama, Y.; Gu, J. Microbial Community Analysis of Fresh and Old Microbial Biofilms on Bayon Temple Sandstone of Angkor Thom, Cambodia. *Microb. Ecol.* **2010**, *60*, 105–115. [[CrossRef](#)] [[PubMed](#)]
44. Kusumi, A.; Li, X.; Osuga, Y.; Kawashima, A.; Gu, J.; Nasu, M.; Katayama, Y. Bacterial Communities in Pigmented Biofilms Formed on the Sandstone Bas-Relief Walls of the Bayon Temple, Angkor Thom, Cambodia. *Microbes Environ.* **2013**, *28*, 422–431. [[CrossRef](#)] [[PubMed](#)]
45. Mase, Y.; Rouborn, W.J.; Quackenbush, F.W. Carotene production by *Penicillium sclerotiorum*. *Arch. Biochem. Biophys.* **1957**, *68*, 150–156. [[CrossRef](#)]
46. Butler, M.; Day, A. Fungal melanins: A review. *Can. J. Microbiol.* **1998**, *44*, 1115–1136. [[CrossRef](#)]
47. Elbaghdady, K.Z.; Tolba, S.T.; Houssien, S.S. Biogenic deterioration of Egyptian limestone monuments: Treatment and conservation. *J. Cult. Herit.* **2019**, *38*, 118–125. [[CrossRef](#)]
48. Gaylarde, P.M.; Gaylarde, C.C. Algae and cyanobacteria on painted surfaces in Southern Brazil. *Rev. Microbiol.* **1999**, *30*, 209–213. [[CrossRef](#)]
49. Alexander, S.; Schiesser, C.H. Heteroorganic molecules and bacterial biofilms: Controlling biodeterioration of cultural heritage. *ARKIVOC* **2017**, *2017*, 180–222. [[CrossRef](#)]
50. Martino, P.D. What About Biofilms on the Surface of Stone Monuments? *Open Conf. Proc. J.* **2016**, *6*, 14–28. [[CrossRef](#)]
51. Erbehtas, A.R.; Isgor, O.B.; Weiss, W.J. Comparison of Chemical and Biogenic Acid Attack on Concrete. *ACI Mater. J.* **2020**, *117*, 255–264. [[CrossRef](#)]
52. Charola, A.E.; Puhlinger, J.; Steiger, M. Gypsum: A review of its role in the deterioration of building materials. *Environ. Geol.* **2007**, *52*, 207–220. [[CrossRef](#)]
53. Coccato, A.; Moens, L.; Vandenabeele, P. On the stability of mediaeval inorganic pigments: A literature review of the effect of climate, material selection, biological activity, analysis and conservation treatments. *Herit. Sci.* **2017**, *5*, 70. [[CrossRef](#)]
54. Sterflinger, K.; Pinar, G. Microbial deterioration of cultural heritage and works of art-tilting at windmills? *Appl. Microbiol. Biot.* **2013**, *97*, 9637–9646. [[CrossRef](#)] [[PubMed](#)]
55. Aviam, O.; Bar-Nes, G.; Zeiri, Y.; Sivan, A. Accelerated biodegradation of cement by sulfur-oxidizing bacteria as a bioassay for evaluating immobilization of low-level radioactive waste. *Appl. Environ. Microb.* **2004**, *70*, 6031–6036. [[CrossRef](#)] [[PubMed](#)]
56. Markou, G.; Georgakakis, D. Cultivation of filamentous cyanobacteria (blue-green algae) in agro-industrial wastes and wastewaters: A review. *Appl. Energy* **2011**, *88*, 3389–3401. [[CrossRef](#)]
57. Ortega-Calvo, J.J.; Arino, X.; Stal, L.J.; Saiz-Jimenez, C. Cyanobacterial sulfate accumulation from black crust of a historic building. *Geomicrobiol. J.* **1994**, *12*, 15–22. [[CrossRef](#)]
58. Brueckner, R.; Williamson, S.J.; Clark, L.A. The effects of the thaumasite form of sulfate attack on skin friction at the concrete/clay interface. *Cem. Concr. Res.* **2012**, *42*, 424–430. [[CrossRef](#)]
59. Ma, W.; Wu, F.; Tian, T.; He, D.; Zhang, Q.; Gu, J.; Duan, Y.; Ma, D.; Wang, W.; Feng, H. Fungal diversity and its contribution to the biodeterioration of mural paintings in two 1700-year-old tombs of China. *Int. Biodeter. Biodegr.* **2020**, *152*, 104972. [[CrossRef](#)]
60. Lajili, H.; Devillers, P.; Grambin-Lapeyre, C.; Bournazel, J.P. Alteration of a cement matrix subjected to biolixiviation test. *Mater. Struct.* **2008**, *41*, 1633–1645. [[CrossRef](#)]

61. Michael, G.; Bahri-Esfahani, J.; Li, Q.; Rhee, Y.J.; Wei, Z.; Fomina, M.; Liang, X. Oxalate production by fungi: Significance in geomycology, biodeterioration and bioremediation. *Fungal Biol. Rev.* **2014**, *28*, 36–55.
62. Sabbioni, C.; Ghedini, N.; Bonazza, A. Organic anions in damage layers on monuments and buildings. *Atmos. Environ.* **2003**, *37*, 1261–1269. [[CrossRef](#)]
63. Fomina, M.; Burford, E.P.; Hillier, S.; Kierans, M.; Gadd, G.M. Rock-Building Fungi. *Geomicrobiol. J.* **2010**, *27*, 624–629. [[CrossRef](#)]
64. Sanchez-Silva, M.; Rosowsky, D.V. Biodeterioration of Construction Materials: State of the Art and Future Challenges. *J. Mater. Civ. Eng.* **2008**, *20*, 352–365. [[CrossRef](#)]
65. Scheerer, S.; Ortega-Morales, O.; Gaylarde, C. Microbial deterioration of stone monuments—An updated overview. *Adv. Appl. Microbiol.* **2009**, *66*, 97–139. [[PubMed](#)]
66. Gaylarde, P.; Gaylarde, C. Algae and cyanobacteria on painted buildings in Latin America. *Int. Biodeter. Biodegr.* **2000**, *46*, 93. [[CrossRef](#)]